Modeling of the Dynamic-Bulging-Induced Surface Level Fluctuations in Continuous Casting

Zhengtao Xu[1], Zhelin Chen[1], Lu Chen[1], Bryan Petrus[2], Madison Milligan[2], Daniel Stephens[2], Joseph Bentsman[1], Brian G. Thomas[3],

[1]University of Illinois at Urbana-Champaign

1206 W Green St, Urbana, IL, USA, 61801

[2]Nucor Steel Decatur

4301 Iverson Blvd. Trinity, AL, USA, 35673

[3]Colorado School of Mines

1610 Illinois St, Golden, CO, USA, 80401

Email: bgthomas@mines.edu

Key Words: continuous casting, dynamic bulging, frozen fraction, heuristic geometric modification, shell thickness, shell profile

ABSTRACT

Mold level fluctuations in continuous casting of steel slabs give rise to slag inclusions, strand surface cracks, and, in severe cases, breakouts. One of the main causes of mold level fluctuations is dynamic bulging, which arises due to periodic squeezing of the strand in the spray cooling zones beneath the mold. This paper presents two models to predict the effect of dynamic bulging on liquid level variations. The first model estimates mold level variations due to dynamic bulging based on two submodels: 1) a computational heat flow model of the continuous casting process that outputs strand surface temperature and shell thickness to an empirical equation to estimate the maximum inner-roll bulging amplitude under steady casting conditions, and 2) an analytical geometric model that calculates the dynamic shape of the bulged shell and the resulting mold level fluctuations, based on the output from the first model and an assumed frozen fraction history. The second model is a simple analytical calculation of the dynamic bulging effect based on the difference between two plant measurements: the mold level sensor data and the stopper rod position, together with a model that predicts the effect of inlet flow variations from the tundish through the SEN into the mold under transient conditions, caused by the measured stopper rod movements, including the effects of erosion. The predictions from these two models are compared to gain new insight into the mold level fluctuations caused by dynamic bulging. At present, this comparison shows quantitative similarities, but also noticeable discrepancy. Steps to improve the accuracy of both models are discussed.

INTRODUCTION

The quality of steel manufactured by continuous casting depends on controlling many different phenomena. Perhaps the most important factor affecting steel quality is ability to control transient fluctuations of the mold level. These fluctuations lead to severe quality problems, such as surface defects and the entrainment of mold slag that forms the inclusions. Level fluctuations also lead to large, detrimental slag rims, which prevent proper liquid mold slag infiltration. Severe mold level fluctuations also cause deep oscillation marks and increase the incidence of surface cracks [1], [2] and the chance of breakouts [3]. Currently,

mold level control is performed by a single actuator, such as the stopper rod, or the slide gate, the position of which controls the metal flow rate into the mold. These flow rate actuators at best can maintain the average liquid level in the mold, but they cannot prevent mold level fluctuations, which depend on turbulent fluid flow and other phenomena. The stopper rod system cannot fully compensate the severe mold level oscillation. Among the other phenomena leading to mold level fluctuation, dynamic bulging is an important one that is not yet understood sufficiently well [3].

Bulging refers to the outward convex deformation of the solidifying steel shell between the supporting rolls in the secondary spray cooling zones of a continuous slab caster [4]. The simplified illustration of bulging is depicted in Figure 1, where the shell waviness is exaggerated for clarity.

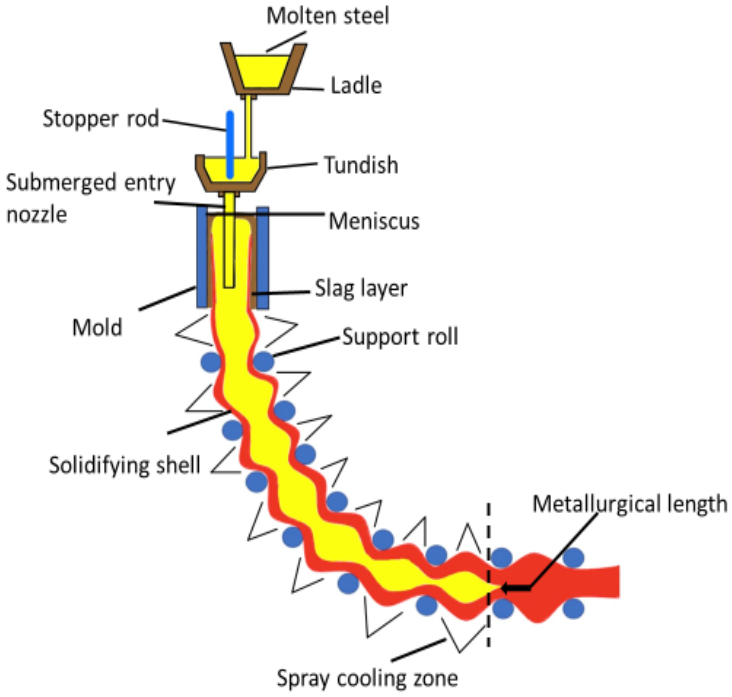

Figure 1. Illustration of a continuous casting process with the bulged shell.

Bulging is unavoidable due to the soft, creep-sensitive properties of the solidifying steel shell subject to the internal ferrostatic molten steel pressure, which pushes the shell outwards as the latter grows and moves down the caster [3], [4]. When bulging is excessive, the cast steel quality may be negatively impacted by the bulging deformation itself. However, the biggest adverse effect of bulging on continuous casting process is in producing the transient changes in the molten steel containment shape in the strand, which further translate into dynamic changes in the mold level. Indeed, due to the molten steel incompressibility, any dynamic change in the shell shape is almost instantaneously converted into the mold level change. The latter forces the flow-control system to compensate for it by manipulating the liquid steel volume in the entire mold/strand cavity through the flow rate change. This dynamical coupling of the strand bulging with the mold level often leads in practice to major steel quality problems due to excessive mold level fluctuations.

The purpose of this paper is to present a comparative system to predict and evaluate dynamic bulging due to the time-varying geometry of the moving strand in the continuous steel caster and its corresponding effect on fluid volume, containment shape, and mold level fluctuations. The main intended use of this system is to guide the development of a more accurate dynamic bulging model and on its basis the design of an optimized control system for simultaneous mold level and spray-cooling control to mitigate the bulging effects on steel quality.

Dynamic bulging can be considered to have two extreme types of behavior. The first extreme is steady or static bulging, which causes "snaking" of the shell down the strand between the support rolls. This snake shell scenario takes place when the outer surface of the solidifying steel shell exactly follows the previous shell shape down through the rolls, progressing thereby along the exact same path. Namely, while the shell surface continuously undergoes transverse oscillation as it bulges back and forth between rolls from the perspective of the material motion (Langrangian reference frame), the shape of the shell from the perspective of the caster itself (Eulerian reference frame) remains unchanged with time.

The other extreme type of bulging is when the local shell shape becomes fully frozen, losing its ability to bend around between the rolls. As the frozen shell moves down along the casting direction, the previously-bulged regions are squeezed beneath the rolls, causing large changes in the shape of the contained liquid volume and leading to severe oscillations in the mold level.

Neither the snake shell, nor the frozen shell extreme scenarios are likely to happen in a real caster. Instead, some intermediate state occurs, which comprises the real dynamic bulging behavior [5]. Depending on the rate of creep in the strand and events encountered by the locally moving strand, such as a change in a roll pitch, the shell will become partially frozen. As a given portion of this partially rigid shell continues to move down the caster under the influence of the ferrostatic pressure and the rolls rotation, its transverse variations will not exactly follow the path of the previous downstream shell. Instead, regions of less convex, or even concave shape with respect to the rolls will be generated, leading to the transvers shell oscillations and the resulting mold level variations of interest in this work. Prediction of this behavior presents a significant modeling challenge.

To address the task of estimating the effect of dynamic bulging on the mold level, the present effort uses two models, based, respectively, on analytical/numerical calculation and on plant measurements. The first model includes two sub-models. The first sub-model, ConOffline [6], [7], provides the 2D longitudinal shell temperature and thickness profile in the entire caster by interpolating a series of 1D moving slices. This sub-model is used to provide thermal input data to an empirical equation to calculate the maximum inner-roll bulging amplitude under steady casting conditions [4]. The second sub-model uses a geometric representation of the bulging deformation itself [2]. Using the bulging amplitude from the first sub-model and the previous calculation, as well as setting the frozen fraction history to account for the creep deformation and other phenomena, the second sub-model calculates the dynamic bulging, or shape evolution of the entire surface of the strand in the caster with time and an estimate of the mold level variations due only to dynamic bulging.

The second model calculates the residual mold level fluctuations arising solely due to dynamic bulging. To accomplish this, it employs the time-varying mold level and the stopper rod position signals: two quantities measured at the caster, in addition to a model that calculates the effect of stopper rod movement on inlet flow variations based on predicted pressure variations [8]. Results predicted from both models are compared and used for evaluating dynamic bulging and for model improvement. The sequential steps in the usage of both models are described in the next section.

At present, when severe dynamic bulging is detected, a steel company will typically increase the spray cooling rate within some of the spray zones along the strand until bulging is diminished. However, this trial-and-error technique of bulging elimination is empirical, and its inner working, even when successful, is unclear, and likely non-optimal from an overall casting quality standpoint. Thus, the goal of the current work is to develop a fundamental system of models to predict the phenomenon, validate it with plant measurements, apply it to improve understanding of dynamic bulging, and finally to develop a better technique to lessen the effects of dynamic bulging and to thereby improve steel quality.

COMPARATIVE BULGING MODELING SYSTEM

This paper presents the first comparative system for bulging modeling. The purpose of this system is to compare the mold level estimates based on an analytical/numerical bulging model with those based on plant measurements to guide the bulging model improvement. The system employs two models. The first one is based on the analytical and numerical modeling of the bulging phenomenon itself. It includes two sub-models: 1) a computational heat flow model of the continuous casting process for calculating the maximum inner-roll bulging amplitude under steady casting conditions, and 2) a geometric model for calculating the bulging deformation and the resulting mold level fluctuation estimate based on the output from the first model and an assumed frozen fraction history. The second model does not employ any analytical bulging description, but rather uses the 1) mold level sensor data measured at the caster, 2) the history of stopper rod position measured at the caster, and 3) a model

developed in previous work to relate the variations in liquid flow rate from the tundish through the SEN and into the mold under transient conditions, to the stopper position, including the effects of erosion. This second model then estimates the effect of bulging on the mold level. Using this new setting, the mold level fluctuations predicted by the first model are compared with those calculated by the second model.

The first model in this comparative system is presented in terms of a sequence of steps in the left-side diagram in Figure 2a. The first step in this model is to calculate the temperature and the shell-thickness profile down the caster. This step is provided by a calibrated heat transfer solidification model, ConOffline. The second step employs the analytical static nonlinear relation to compute the magnitude of the maximum bulging between the rolls using the surface temperature and shell thickness profiles calculated from the previous step. Finally, the dynamic shape of the bulged shell is used to determine the time-variation of the volume shape of the entire liquid pool, and the corresponding variation in the mold level due to bulging. The second step of the first model is presented schematically with more detail in Figure 2b.

As seen in the right-side diagram in Figure 2a, the second model uses the mold level sensor data and the stopper rod position, both measured at the caster, on their basis calculates the bulging volume variation, and further on, computes the average mold liquid level variations due to bulging.

The mold level variations computed by both models are compared to guide modeling improvement – the subject of the future work.

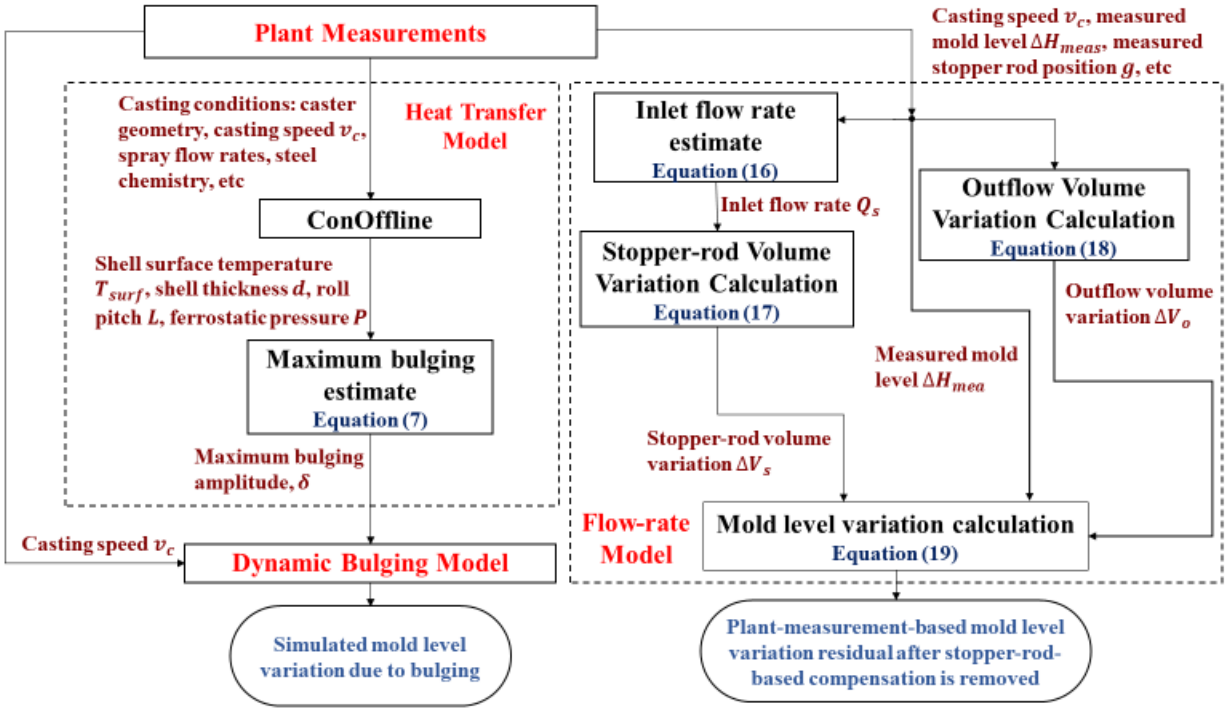

Figure 2a. Comparative bulging modeling system: the left-side diagram depicts an analytical/numerical model of dynamic bulging; the right-side diagram depicts a corresponding model based on plant data – measured mold level and measured stopper rod position. Outputs from both models are compared and used for subsequent model improvement.

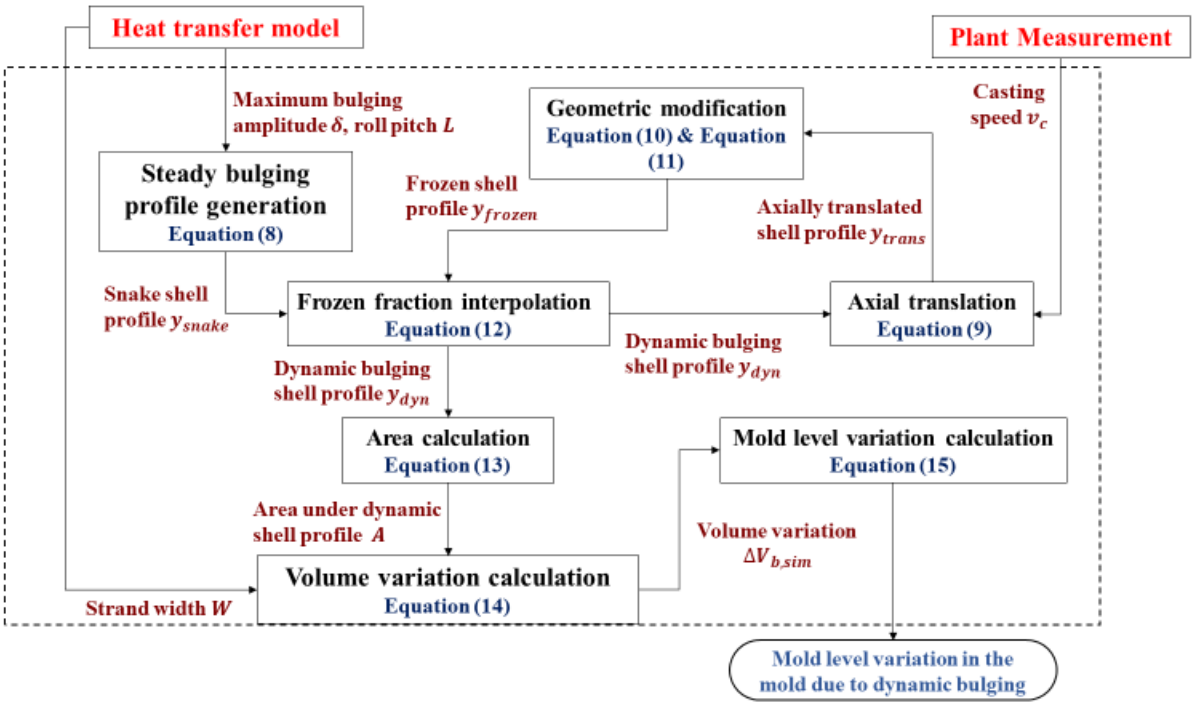

Figure 2b. Illustration of the dynamic bulging sub-model in the first model.

A description of both models depicted in Figure 2a and Figure 2b along with the corresponding variables is given below.

Model 1 Step 1) Heat transfer and steady bulging profile

The amplitude of the steady bulging shell profile down the caster is needed as the first step to simulate dynamic bulging. For this purpose, shell thickness and temperature distribution along the steel strand are first calculated by ConOffline, an offline version of ConOnline [9] derived from the previous work [7], [10]–[13]. ConOffline uses explicit finite-difference method in a Lagrangian reference frame to solve the transient heat-conduction equation within transverse slices moving in the z direction at casting speed [14]. For each slice, the following equations are solved:

$$\rho c_p^* \frac{\partial T}{\partial t} = \frac{\partial}{\partial x}(k \frac{\partial T}{\partial x}), \tag{1}$$

where x is the thickness direction – domain of a single 1D slice, T is temperature, ρ is density, k is thermal conductivity, and c_p^* is effective specific heat, which depends on the latent heat of fusion, L_f, and the solid fraction, f_s:

$$c_p^* = c_p + L_f \frac{df_s}{dT}. \tag{2}$$

The boundary conditions are the heat flux leaving the strand surface, $q(t)$. In the mold, surface heat flux is based on measurements by Duvvuri conducted on this caster [15]:

$$q(t) = Q_m[MW/m^2] = 1.197(v_c[m/min])^{0.544}, \tag{3}$$

where v_c is the casting speed. Below the mold, spray cooling heat flux is based on a relation from Nozaki [16], based on measurements on this caster:

$$q(t) = AQ_{water}(MW/m^2)^c(T(0,t) - T_\infty), \tag{4}$$

where Q_{water} is the local water spray flux, A and c are fitting parameters based on plant measurements, $T(0,t)$ is the surface temperature, T_{surf} , and T_∞ is the temperature of the spray cooling water. Assuming two-fold symmetry, the strand centerline is insulated:

$$\frac{\partial T}{\partial x}(L,t) = 0. \tag{5}$$

For the initial condition, the molten steel temperature in the mold is set to the pour temperature, T_{pour} .

$$T(x,0) = T_{pour}. \tag{6}$$

ConOffline simulates N slices simultaneously, covering the entire secondary cooling zone. For the simulation in this work N=200 is used, but this number can be adjusted to meet other resolution requirements [6]. Yu's equation [4] is employed to compute the maximum bulging amplitude, $\delta_{\max}$,

$$\delta_{\max}(mm) = 7.1496\times10^{-34}\frac{L_{(mm)}^{6.5}P_{(MPa)}^{1.993}T_{surf(^\circ C)}^{8.766}}{d_{(mm)}^{5.333}}, \tag{7}$$

where the local strand surface temperature T_{surf} , the solidified shell thickness d, the roll pitch L, and the ferrostatic pressure P are provided by ConOffline [3]. In this paper, the roll pitch L is assumed identical within each zone.

Model 1 Step 2) Dynamic bulging sub-model and bulging-induced analytical mold level calculation

As noted earlier, the actual dynamic bulging resides between two extreme scenarios: steady bulging (snaking shell) and unsteady bulging (frozen shell) [3]. To bring out the difference between these two bulging types, Figure 3 introduces the concept of the roll pitch liquid steel volume. This volume, denoted as ΔV_c, is the volume of the liquid steel contained in the strand portion between the two adjacent rolls from the inner shell surface to the centerline. Under steady bulging the shell does not undergo any transverse displacement because of its compliance with the shape formed. However, when the shell solidifies to a higher degree, it loses compliance, and the resulting bulge travels downstream, pushing against the downstream roll, and forcing the shell to move inwards, This partial shell freezing then creates the transverse oscillatory motion of the shell and the resulting oscillatory change in the roll pitch liquid steel volume. This change is then directly translated into the corresponding change in the liquid steel volume in the mold, moving the level of the liquid steel in the mold up or down.

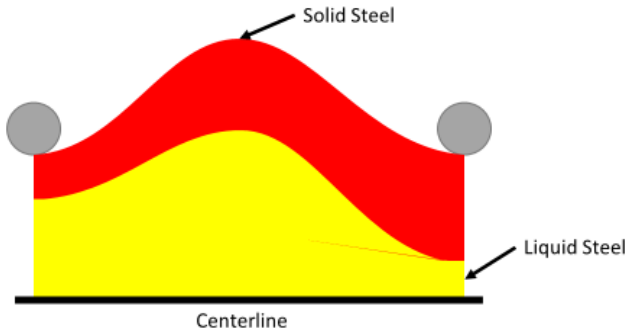

Figure 3. Illustration of the roll pitch liquid steel volume in the secondary cooling zone.

Thus, the "snake shell" (left) produces no steel volume changes in the mold and hence no level fluctuations, while the unsteady "frozen shell" (right) is expected to produce the most roll pitch steel volume changes and consequent detrimental mold level fluctuations. To investigate realistic behavior, the "frozen fraction" concept is introduced, which linearly interpolates between these two extremes in a prescribed manner according to the expected events in the strand history. Specifically, the frozen fraction function, $f(z,t)$, is defined as a time and position-dependent parameter that varies between 0 and 1. When the frozen fraction equals to 0, the shell experiences the steady bulging. At the other extreme, when the frozen fraction is 1, the shell exhibits completely frozen behavior, which is termed a 'frozen shell'. This behavior is shown in Figure 4.

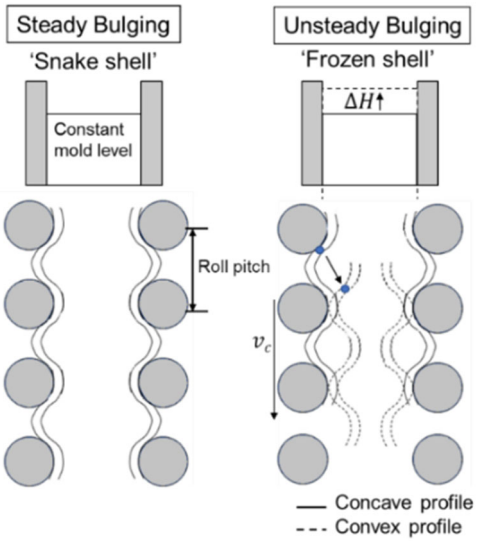

Figure 4. Illustration of snake shell and frozen shell [3].

To model dynamic bulging behavior, the following assumptions are made:

(A1) The steady bulging shell profile has a sinusoidal waveform between each pair of rolls.

Based on assumption (A1), the snake shell profile is generated by concatenating at the locations of rolls the full sinusoid cycles independently generated between each pair of rolls. The amplitude of each sinusoid cycle is set to the maximum bulging amplitude calculated by ConOffline at each time step. The snake shell profile $y_{snake}(z,t)$ for each roll pitch is described as:

$$y_{snake}(z,t) = -\frac{\delta_{\max}(t)}{2}(\cos(2\pi\frac{z-z_{up}}{L})+1), \tag{8}$$

where $\delta_{\max}(t)$ is the maximum bulging amplitude at each time step calculated from Eq. (7), z is the position starting at the mold exit, and z_{up} is the location of the upstream roll. Figure 5 indicates the generation of steady bulging profile between a pair of rolls. The entire snake shell profile is formed by connecting the snake shell profiles of each roll pitch.

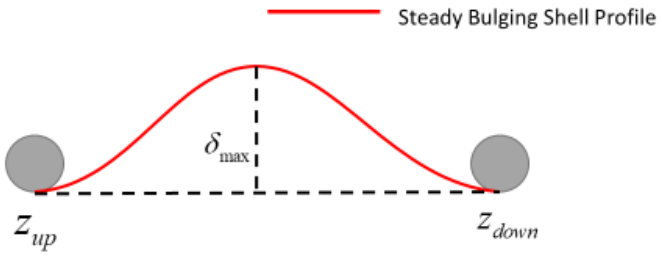

Figure 5. Illustration of the steady bulging profile generation.

(A2) The dynamic shell profile moves down the caster, maintaining its shape, while always keeping contact with every roll, owing to the internal ferrostatic pressure.

At each time step, a new frozen shell profile is computed based on the dynamic bulging shell profile at the previous time step. As the shell profile moves one time step along the casting direction, the perfectly frozen bulging profile $y_{frozen}(z,t)$ is generated based on assumption (A2). The axially translated shell profile $y_{trans}(z,t)$ is adjusted as follows to find the frozen shell bulging profile:

$$y_{trans}(z,t) = y_{dyn}(z - v_c(t)\cdot\Delta t,\ t-\Delta t), \tag{9}$$

where t is the time and Δt is the time step. As shown by the black solid line in Figure 6, the dynamic bulging shell profile, $y_{dyn}(z,t-\Delta t)$, from the previous time step (defined later in Eq. 12) is moved axially at the casting speed for one time step to form the axially translated shell profile, y_{trans}.

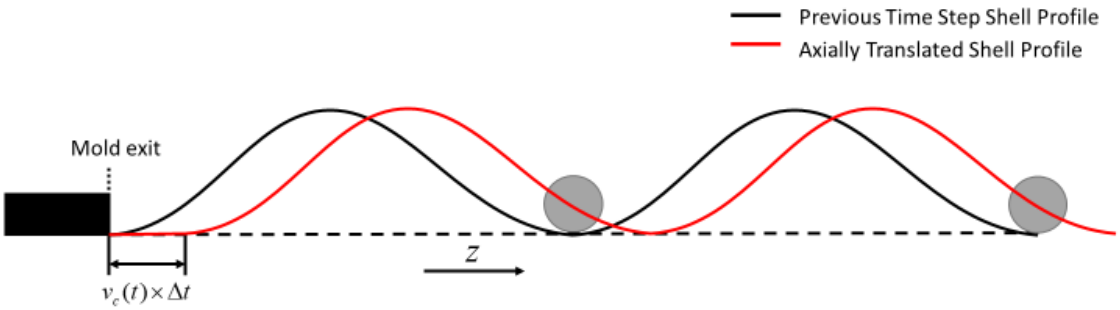

Figure 6. An unrealistic axially translated frozen shell profile.

To satisfy Assumption A2, a geometric modification is introduced to avoid the unrealistic profile, y_{trans}, as illustrated in Figure 6. Starting at the last roll pitch at the exit of the caster, Figure 7a shows the geometric modification of the shell surface profile between a typical pair of rolls. The profile is shifted perpendicularly to the axial direction (casting direction) in order to exactly touch the downstream roll. Figure 7b shows the last step of the modification process between the mold exit and the first roll. This process generates the following "modification curve", h:

$$h(z,t) = y_{trans}(z_{up},t) + \frac{y_{trans}(z_{down},t) - y_{trans}(z_{up},t)}{L}(z - z_{up}), \tag{10}$$

where z_{up} is the axial position of the upstream roll, z_{down} is the axial position of the downstream roll, $y_{trans}(z_{up},t)$ is the perpendicular height of the axially translated shell profile with respect to the bottom of the upstream roll, and $y_{trans}(z_{down},t)$ is the perpendicular height of the axially translated shell profile with respect to the bottom of the downstream roll.

Next, subtracting the modification curve from the axially translated shell profile repositions the resulting shell profile to touch every roll and form the new frozen shell profile, calculated for every roll pitch as:

$$y_{frozen}(z,t) = y_{trans}(z,t) - h(z,t)\,. \tag{11}$$

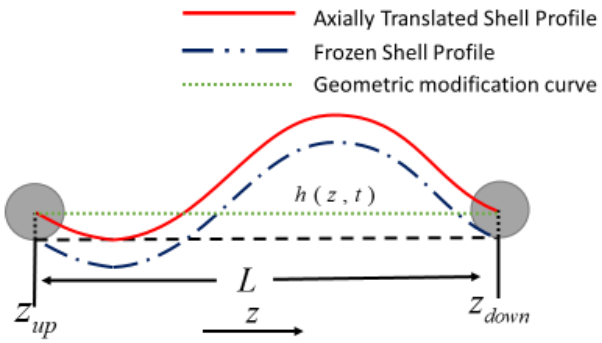

Figure 7a. Illustration of the geometric modification process between two rolls.

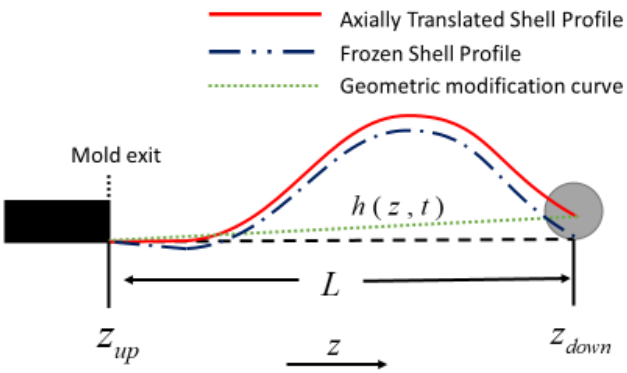

Figure 7b. Illustration of the geometric modification process between the mold exit and the roll.

The dynamic bulging shell $y_{dyn}(z,t)$ is then calculated as a linear weighted aggregation of the snake shell and the new frozen shell:

$$y_{dyn}(z,t) = (1 - f(z,t)) \times y_{snake}(z,t) + f(z,t) \times y_{frozen}(z,t), \tag{12}$$

where z is the position downstream from the mold exit, t is time, Δt is the time step, y_{snake} is the snake shell profile, and y_{frozen} is the frozen shell profile. Figure 8 shows an example of a dynamic bulging shell profile for two roll pitches, with frozen fraction equal to 0.5.

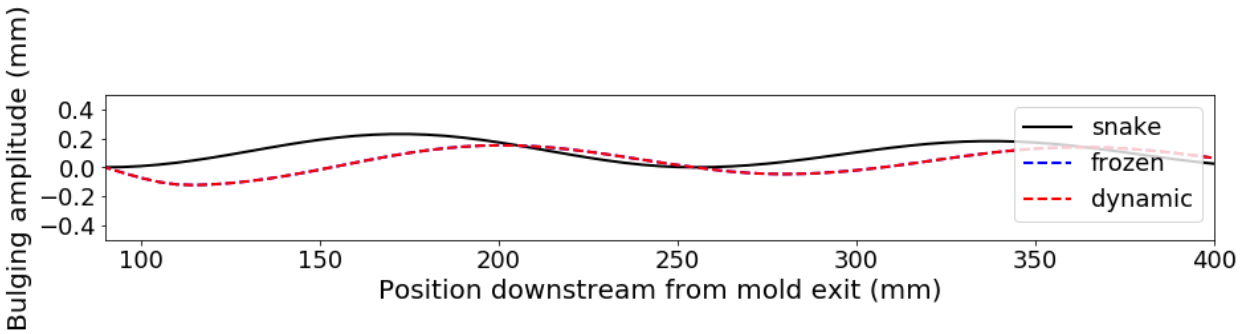

Figure 8. Illustration of the formation of the dynamic bulging profile when the frozen fraction is 0.5.

To compute the time evolution of the area variation between the inner shell surface and the centerline due to dynamic bulging, the area $A(t)$ between the inner shell profile and the centerline needs to be calculated at each time step. The latter task is, however, greatly simplified for the following reason. In a bulged shell, the inner shell surface has roughly the same shape as the outer shell surface. At the metallurgical length, the inner shell surface vanishes since all the liquid steel between it and the centerline has been solidified. Thus, beyond this point, the bulging amplitude no longer affects the liquid pool. However, because the transverse shell displacement amplitude due to bulging is extremely small, the effect of this displacement extends all the way up to the metallurgical length, giving rise to the area calculation of the form

$$A(t) = \int_0^{ML} y_{dyn}(z,t)dz, \tag{13}$$

i.e., with the upper limit taken to be the metallurgical length of the steel ML.

The decreasing area under the 2D shell profile of Figure 3 causes the volume contained between the two shells on opposite sides of the strand part in the containment zone to decrease. To conserve the total volume of the incompressible molten steel in the liquid cavity, the excess volume of molten steel pushes the liquid level upward inside the mold. Therefore, the volume variation due to the simulated dynamic bulging $\Delta V_{b,sim}$ is computed at each time step:

$$\Delta V_{b,sim}(t) = -2W(A(t) - A_0), \tag{14}$$

where W is the width of the strand and A_0 is the area under the initial bulging shell profile. Assuming that this volume variation is equal to the volume variation in the mold, but with the opposite sign, and the mold cross-section area is A_s, the mold level variation $\Delta H_{sim}(t)$ due to dynamic bulging from simulation can be calculated using the relationship:

$$\Delta H_{sim}(t) = \Delta V_{b,sim}(t) / A_s . \tag{15}$$

Model 2: Bulging-induced mold level model based on measured mold level and stopper rod position

A pressure-drop/flow-rate model for the stopper rod system (PFSR) is adopted to predict the flow rate of molten steel into the caster from the tundish and down through the nozzle [3]. Details of PFSR can be found in [8]. During the casting process under investigation in this work, the stopper rod tip experiences erosion due to the calcium treatment of the molten steel. To account for the erosion effect on the inlet flow rate, the following empirical linear equation is introduced [3]:

$$Q_s(t) = 0.5925g(t) + 0.764 , \tag{16}$$

where Q_s (ton/min) is the inlet flow rate and $g(t)$ (mm) is the stopper rod vertical incremental movement. The slope and the y-intercept are empirical constants, calibrated from measurements at this caster, and taking into account slow erosion of the stopper tip due to the calcium treatment [3].

The volume variation in the mold depends on inlet flow, outlet flow, and dynamic bulging. To calculate the volume variation due to bulging only, the other volume variations need to be considered. The volume change due to inlet flow from the tundish ΔV_s can be calculated as:

$$\Delta V_s(t) = Q_s(t) \cdot \Delta t \,. \tag{17}$$

The outlet steel flow speed is measured and taken to represent the casting speed v_c. The dimensions of the mold are given. The volume changes due to outflow ΔV_o can be calculated as:

$$\Delta V_o(t) = W_m D_m v_c(t) \rho \Delta t \,, \tag{18}$$

where W_m is the width of the mold, D_m is the length of the mold, and ρ is the density of the molten steel. The mold level variation due to dynamic bulging only, $\Delta H_{est}(t)$, based on the plant measurement from the mold level sensor and the calculated inlet and outlet flows is then given as follows:

$$\Delta H_{est}(t) = \Delta H_{meas}(t) - \Delta V_s(t) / A_s + \Delta V_0(t) / A_s \,, \tag{19}$$

where ΔH_{meas} is the measured mold level position, and A_s is the cross-section area of the mold.

PLANT MEASUREMENTS

This section presents the plant measurements of the case under consideration. The data for this case is taken over the time interval of 0-5692 seconds. The corresponding plant measurements of casting speed, stopper rod position, and mold level position are shown in Figures 9 - 11. The casting speed history of the case considered is shown in Figure 9. The average casting speed is 3.09 m/min. The measured stopper rod position is shown in Figure 10. Figure 11 presents the mold level position measured by the mold level sensor.

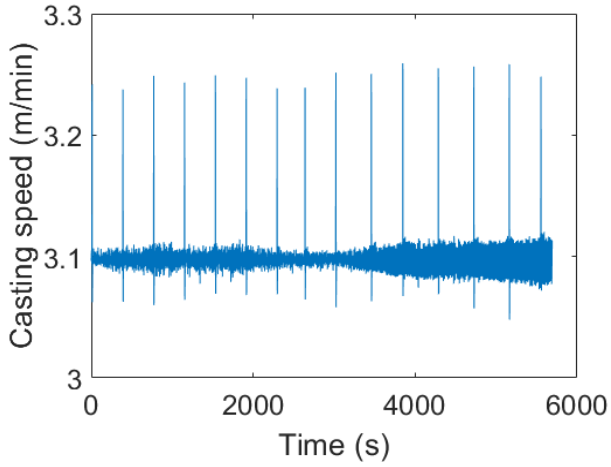

Figure 9. Measured casting speed history.

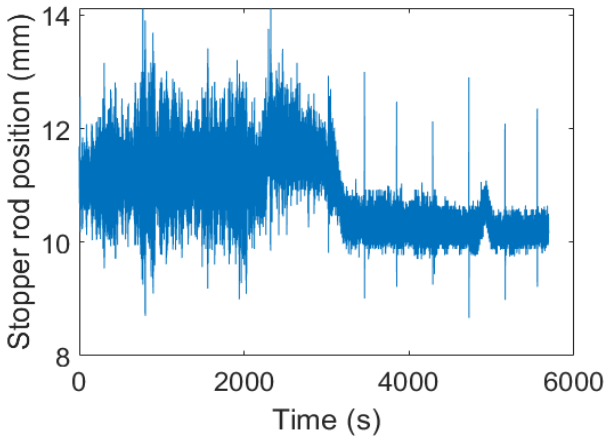

Figure 10. Measured stopper rod position history.

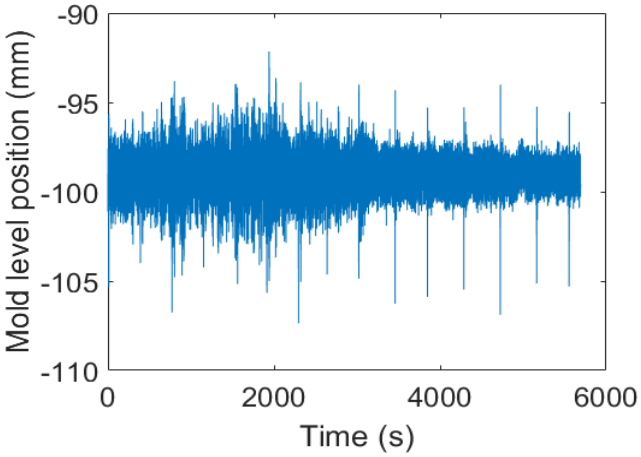

Figure 11. Measured mold level position (raw signal).

SIMULATION RESULTS AND DISCUSSSION

Heat transfer and steady bulging model results

First, the heat transfer model uses the plant measurements to calculate the surface temperature profile and shell thickness profile through ConOffline, as shown in Figure 12. Then, using the calculated results from ConOffline and equations (6) – (7), the steady bulging profile is generated for each time step. Figure 13 shows the generated snake shell profile at the start of the simulation, marked as t=0 seconds.

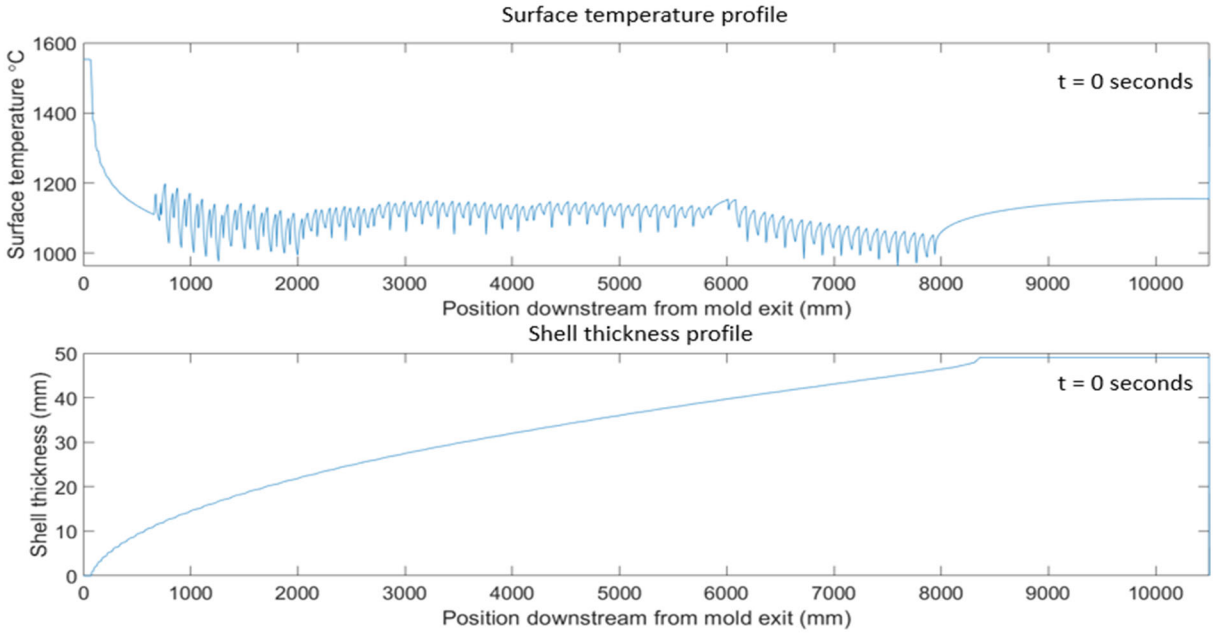

Figure 12. Surface temperature profile and shell thickness profile at the start of the simulation (t = 0 seconds).

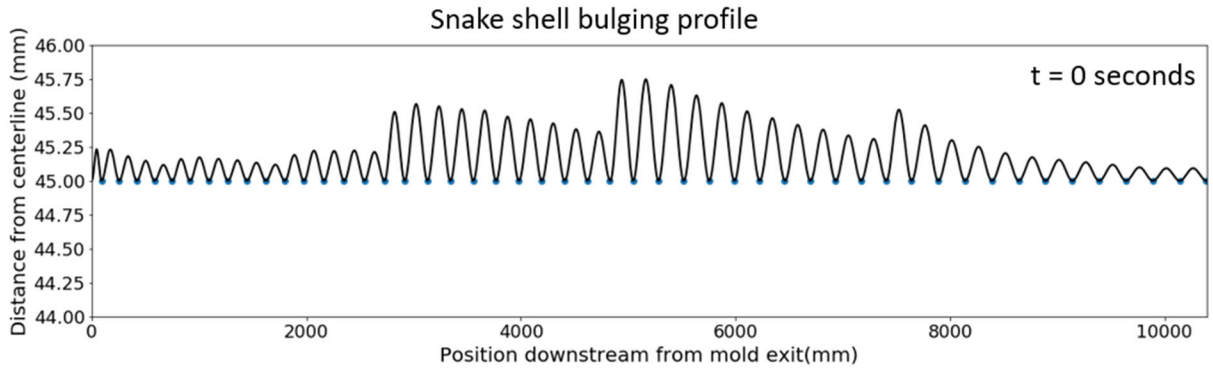

Figure 13. Snake shell profile at the start of the simulation (t = 0 seconds).

Flow-rate / mold level model results

To eliminate the mold level variation effect caused by actions other than bulging, the plant measurements are used as the inputs to the mold level model. Using equations (16) – (19), the mold level model calculates the mold level variation due to dynamic bulging only. The result is shown in Figure 14. The data in Figure 14 is considered to be the measured mold level variation due to dynamic bulging.

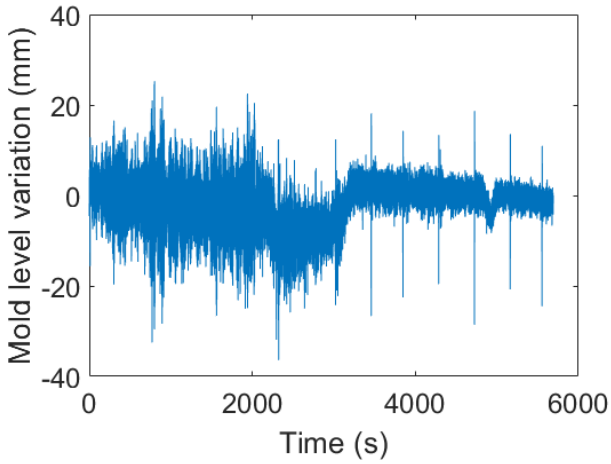

Figure 14. Mold level variation due to bulging only (the residual variation left after subtracting the estimated stopper rod contribution to mold level from the measured mold level history).

Dynamic bulging model results

The simulation of the geometric model uses the required subset of the actual casting speed data. The time step of the simulation is set to be 0.5 s. In this study, the frozen fraction function is set to be a time-independent piecewise function. A frozen fraction of zero (snake shell) is assumed in the first roll pitch in this study. For the rest of the caster, a frozen fraction is set to 1 (perfectly frozen) to investigate an extreme case of dynamic bulging. Figure 15 and Figure 16 are two snapshots of the bulging profile evolution in the simulation. Figure 15 presents the dynamic bulging shell profile which the simulation produces after 2 seconds. Note that the shell profile starting from the second roll pitch has been pushed downwards to the position entirely beneath the rolls. Since the bulging shell is squeezed, it pushes the liquid steel inside the shell back to the mold and causes a level increase in the mold at this time. Figure 16 shows the bulging profile later at 15 seconds. The dynamic bulging shell profile is seen to exhibit both upward and downward radical movements.

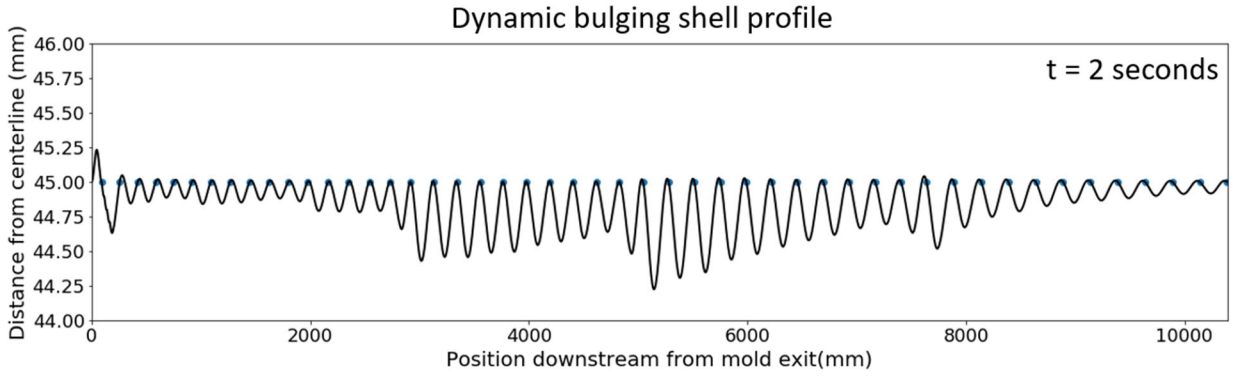

Figure 15. A snapshot of the dynamic bulging shell profile at t=2 seconds.

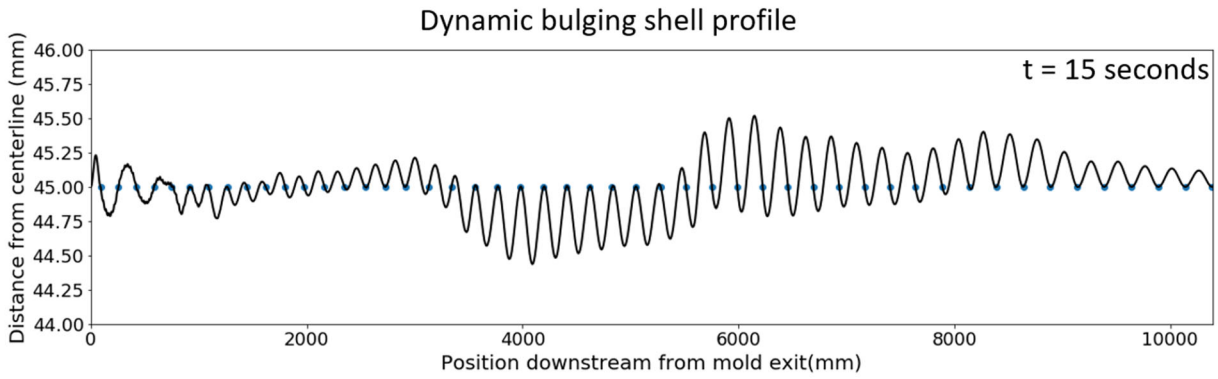

Figure 16. A snapshot of the dynamic bulging shell profile at t=15 seconds.

Mold level results

Figure 17 shows the mold level variation for the first 100 seconds. The mold level starts increasing at t=2 seconds and then drops down. It is physically meaningful, since the shell profile is being squeezed by the rolls as it moves downstream, which is observed in Figure 17. As a result, a portion of the liquid steel inside the shell is being pushed back to the mold and increases the liquid steel level in the mold. The simulated mold level variation oscillates around 36 mm. The amplitude of the mold level variation decreases with respect to time. The maximum difference of the mold level variation from the simulation reaches nearly 70 mm at 2 seconds, as shown in Figure 17. Figure 18 presents the mold level variation due to bulging given by the plant measurements. The maximum difference of the measured mold level variation due to bulging is around 25 mm.

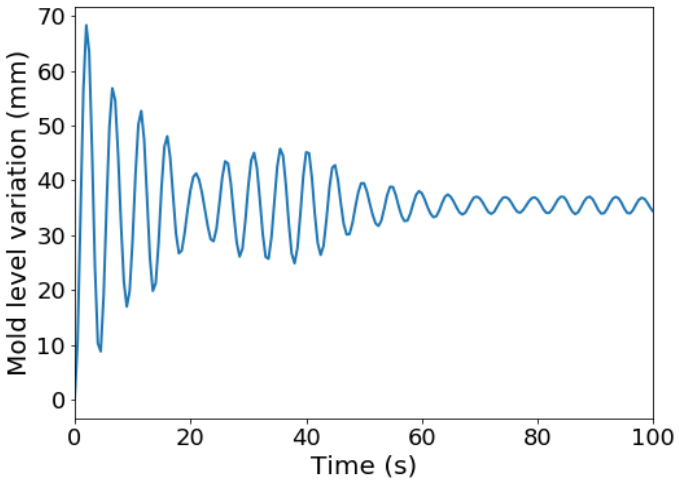

Figure 17. Simulated mold level variation due to bulging only (for 0-100 seconds).

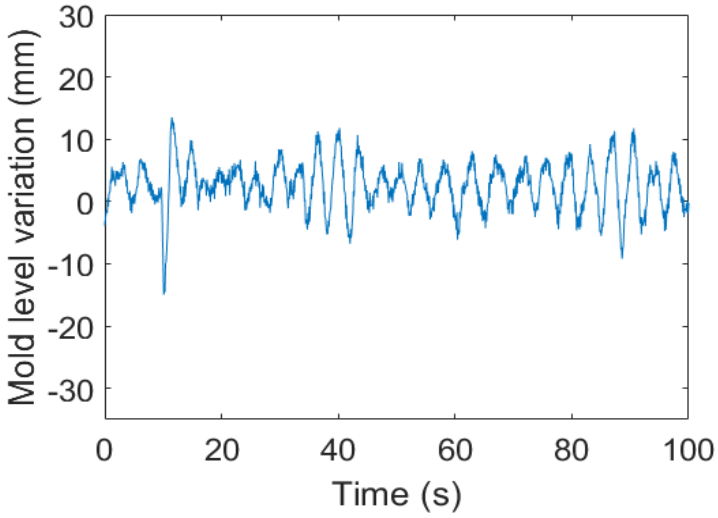

Figure 18. Measured mold level variation due to bulging only for 0-100 seconds (the stopper rod movement effect is subtracted from the measured mold level signal).

A power spectral density (PSD) analysis has been performed for both the measured mold level variation data due to bulging and the simulated mold level bulging-induced variation predictions. The PSD is calculated using Fast Fourier Transformation. The sample interval is chosen to be 200 seconds. The PSD plot of the simulated mold level signal for 0-200 seconds interval is shown in Figure 19. Due to the sample aliasing, the dominant frequency appears close to the frequency of zone 4 and reaches the value of 2.1. There are several peaks seen between the frequency of zone 5 and zone 4. The simulated mold level signal PSD which has the same time window is shown in Figure 20. The dominant frequency is the frequency of zone 8 and the corresponding amplitude is around 3. The PSD of the simulated result does not match the measured one. Further effort is needed to improve the accuracy of the model so that the simulated result matches the data from plant measurements.

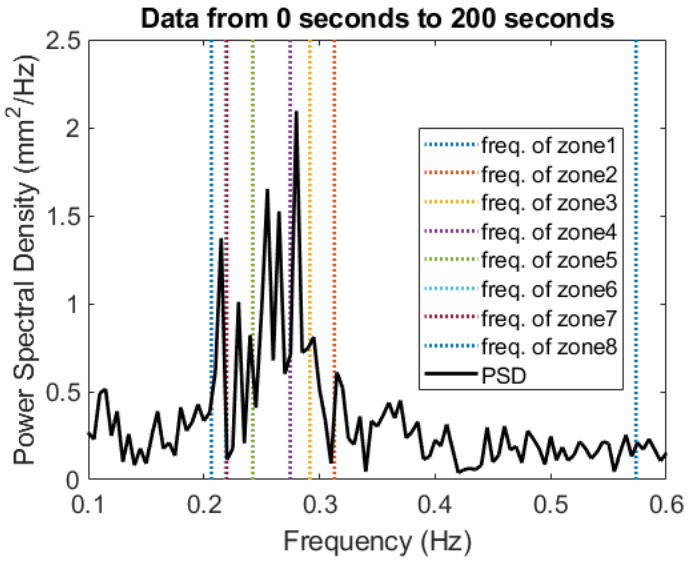

Figure 19. PSD of the measured mold level due to bulging only (with stopper rod effect subtracted).

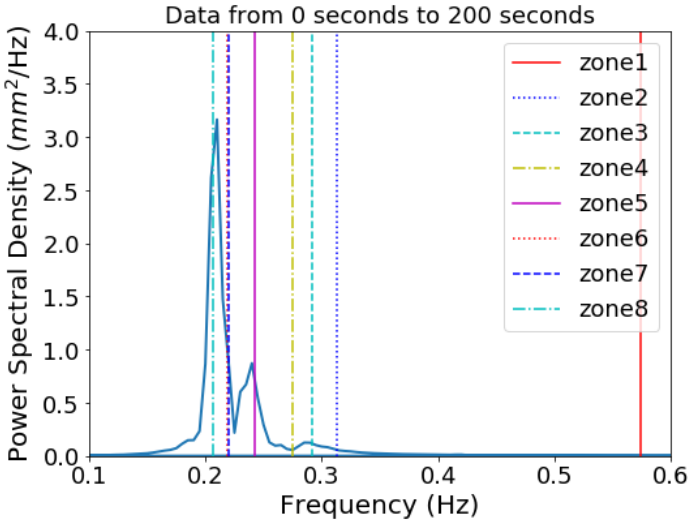

Figure 20. PSD of the simulated mold level due to bulging only for 0-200 seconds.

CONCLUSIONS

A comparative system for dynamic bulging modelling has been developed to study the dynamically-evolving shape of the solidifying steel shell during continuous casting and its effects on severe mold level variations. The system consists of two models, the first one containing two sub-models: heat transfer and steady-bulging amplitude model, and the dynamic bulging model with mold level calculations. These two sub-models are combined to generate the history of the shell profile during dynamic bulging and to compute the evolving shape of the shell profile and the corresponding mold level fluctuations caused only by dynamic bulging. The second model is based on computing mold level fluctuation caused by bulging based on plant measurements of the mold level and the stopper rod position. The simulation results show reasonable quantitative similarities between the outputs of two models. However, additional work is needed to improve the accuracy of the bulging modeling and to incorporate a more realistic frozen fraction description. This work is a preliminary step in understanding and controlling the dynamic bulging phenomenon.

ACKNOWLEDGEMENTS

This work is supported by Nucor Steel Decatur and the Continuous Casting Center at the Colorado School of Mines. Special thanks are extended to Nucor Steel Decatur for continuously providing the plant measurements and caster information.

REFERENCES

[1] G. Mi, J. Zhang, B. Xu, M. Sun, and J. Zhang, “Surface stress evolution and cracks prevention of ingots during the upsetting process,” *Eng. Rev.*, vol. 39, no. 3, pp. 292–301, Jun. 2019, doi: 10.30765/er.39.3.10.

[2] C. Makabe, A. Purnowidodo, and A. J. McEvily, “Effects of surface deformation and crack closure on fatigue crack propagation after overloading and underloading,” *Int. J. Fatigue*, vol. 26, no. 12, pp. 1341–1348, 2004, doi: 10.1016/j.ijfatigue.2004.03.017.

[3] Z. Chen, H. Olia, B. Petrus, M. Rembold, J. Bentsman, and B. G. Thomas, “Dynamic Modeling of Unsteady Bulging

in Continuous Casting of Steel," in *Materials Processing Fundamentals 2019, The Minerals, Metals &Materials Series*, 2019, pp. 23–35, doi: 10.1007/978-3-030-05728-2_3.

[4] L. Yu, "FEM Analysis of Bulging Between Rolls in Continuous Casting," University of Illinois Urbana-Champaign, 2000.

[5] K. Toishi and Y. Miki, "Generation mechanism of unsteady bulging in continuous casting-2 -FEM simulation for generation mechanism of unsteady bulging-," *ISIJ Int.*, vol. 56, no. 10, pp. 1764–1769, 2016, doi: 10.2355/isijinternational.ISIJINT-2016-171.

[6] Z. Chen, W. Drennan, B. G. Thomas, J. Bentsman, and B. G. Thomas, "Investigating Centerline Bridging in Continuous Casting During Speed Drops with ConOffline," in *2019 AISTech - Iron and Steel Technology Conference Proceedings*, 2019, no. May, pp. 2075–2084, doi: 10.1000.377.213.

[7] Z. Chen, J. Bentsman, B. G. Thomas, and A. Matsui, "Study of spray cooling control to maintain metallurgical length during speed drop in steel continuous casting," in *Iron and Steel Technology*, 2017, vol. 14, no. 10, pp. 92–103.

[8] H. Olia and B. G. G. Thomas, "Flow Rate - Stopper Position Model of NUCOR Caster using Pressure Drop Flow Rate Model for Stopper Rod Flow Control Systems (PFSR)," Golden, Co, 2018.

[9] B. Petrus, K. Zheng, X. Zhou, B. G. Thomas, and J. Bentsman, "Real-Time, Model-Based Spray-Cooling Control System for Steel Continuous Casting," *Metall. Mater. Trans. B*, vol. 42, no. 1, pp. 87–103, 2011, doi: 10.1007/s11663-010-9452-7.

[10] B. Petrus, Z. Chen, J. Bentsman, and B. G. Thomas, "Online recalibration of the state estimators for a system with moving boundaries using sparse discrete-in-time temperature measurements," *IEEE Trans. Automat. Contr.*, vol. 63, no. 4, pp. 1090–1096, Apr. 2018, doi: 10.1109/TAC.2017.2736950.

[11] Z. Chen, J. Bentsman, and B. G. Thomas, "Bang-Bang Free Boundary Control of a Stefan Problem for Metallurgical Length Maintenance," in *2018 Annual American Control Conference (ACC)*, 2018, pp. 116–121, doi: 10.23919/ACC.2018.8431904.

[12] Z. Chen, J. Bentsman, and B. G. Thomas, "Enthalpy-based Full-State Feedback Control of the Stefan Problem with Hysteresis," in *58th Conference on Decision and Control (CDC)*, 2019.

[13] B. Petrus, D. Hammon, M. Miller, A. Zewe, B. Williams, Z. Chen, J. Betnsman, B. G. Thomas, "New Method to Measure Metallurgical Length and Application to Improve Computational Models," *Iron Steel Technol.*, vol. 12, no. 12, pp. 58–66, 2015.

[14] Y. A. Meng and B. G. Thomas, "Heat Transfer and Solidification Model of Continuous Slab Casting: CON1D," *Metall. Mater. Trans. B*, vol. 34, no. 5, pp. 685–705, 2003.

[15] P. Duvvuri, B. Petrus, and B. G. Thomas, "Correlation for mold heat flux measured in a thin slab casting mold," in *AISTech - Iron and Steel Technology Conference Proceedings*, 2014, pp. 2881–2893.

[16] T. Nozaki, J. Matsuno, K. Murata, H. Ooi, and M. Kodama, "A Secondary Cooling Pattern for Preventing Surface Cracks of Continuous Casting Slab," *Trans. Iron Steel Inst. Jpn.*, vol. 18, no. 6, pp. 330–338, 1978.